HHS Public Access

Author manuscript

Nat Cell Biol. Author manuscript; available in PMC 2017 February 10.

Published in final edited form as:

Nat Cell Biol. 2016 October ; 18(10): 1043–1053. doi:10.1038/ncb3405.

Interaction between integrin α_5 and PDE4D regulates endothelial inflammatory signalling

Sanguk Yun[1], **Madhusudhan Budatha**[1], **James E. Dahlman**[2,3,4], **Brian G. Coon**[1], **Ryan T. Cameron**[5], **Robert Langer**[2,3,4,6], **Daniel G. Anderson**[2,3,4,6], **George Baillie**[5], and **Martin A. Schwartz**[1,7,8,9]

[1]Department of Internal Medicine, Yale Cardiovascular Research Center, Yale University, New Haven, Connecticut 06520, USA

[2]David H. Koch Institute for Integrative Cancer Research, Massachusetts Institute of Technology, Cambridge, Massachusetts 02139, USA

[3]Harvard-MIT Division of Health Sciences and Technology, Massachusetts Institute of Technology, Cambridge, Massachusetts 02139, USA

[4]Institute for Medical Engineering and Science, Massachusetts Institute of Technology, Cambridge, Massachusetts 02139, USA

[5]Institute of Cardiovascular and Medical Science, College of Medical, Veterinary and Life Sciences, University of Glasgow, Glasgow G12 8QQ, UK

[6]Department of Chemical Engineering, Massachusetts Institute of Technology, Cambridge, Massachusetts 02139, USA

[7]Department of Biomedical Engineering, Yale University, New Haven, Connecticut 06520, USA

[8]Department of Cell Biology, Yale University, New Haven, Connecticut 06520, USA

Abstract

Atherosclerosis is primarily a disease of lipid metabolism and inflammation; however, it is also closely associated with endothelial extracellular matrix (ECM) remodelling, with fibronectin accumulating in the laminin–collagen basement membrane. To investigate how fibronectin modulates inflammation in arteries, we replaced the cytoplasmic tail of the fibronectin receptor integrin α5 with that of the collagen/laminin receptor integrin α2. This chimaera suppressed inflammatory signalling in endothelial cells on fibronectin and in knock-in mice. Fibronectin promoted inflammation by suppressing anti-inflammatory cAMP. cAMP was activated through

[9]Correspondence should be addressed to M.A.S. (martin.schwartz@yale.edu).

AUTHOR CONTRIBUTIONS

S.Y. and M.A.S. designed the project. S.Y. performed *in vitro* experiments and M.B. designed and performed *in vivo* experiments with the aid of S.Y. J.E.D. prepared and provided nanoparticles. B.G.C. contributed PDE4D5 imaging. R.T.C. performed *in vitro* PDE assay. R.L. and D.G.A. provided advice on nanoparticle formulation. S.Y. and M.A.S. wrote the manuscript with the contribution of all the authors.

COMPETING FINANCIAL INTERESTS

The authors declare no competing financial interests.

Note: Supplementary Information is available in the online version of the paper

endothelial prostacyclin secretion; however, this was ECM-independent. Instead, cells on fibronectin suppressed cAMP via enhanced phosphodiesterase (PDE) activity, through direct binding of integrin α5 to phosphodiesterase-4D5 (PDE4D5), which induced PP2A-dependent dephosphorylation of PDE4D5 on the inhibitory site Ser651. *In vivo* knockdown of PDE4D5 inhibited inflammation at athero-prone sites. These data elucidate a molecular mechanism linking ECM remodelling and inflammation, thereby identifying a new class of therapeutic targets.

Atherosclerosis is an inflammatory disease of large to mid-sized arteries that is strongly linked to lipid metabolism[1]. Current concepts and clinical approaches focus mainly on these aspects. However, atherosclerotic plaques occur mainly in regions of arteries with disturbed flow[2,3], which triggers oxidative stress, activation of NF-κB and other mediators, endothelial inflammatory gene expression, and leukocyte recruitment[4]. These local influences synergize with systemic risk factors such as high plasma LDL-cholesterol and triglycerides, hypertension, diabetes or smoking, to induce atherosclerotic plaques[5].

Inflammation and ECM remodelling are closely associated across many biological systems and disease processes[6–8]. Inflammation induces ECM remodelling, with increases in provisional ECM proteins such as fibronectin (FN), osteopontin and fibrin. Conversely, ECM proteins and fragments modulate inflammatory processes. These complex interactions between ECM and inflammatory pathways contribute to normal developmental and adult remodelling, and to a variety of pathologies.

In stable, unperturbed vessels, the subendothelial basement membrane consists mainly of collagen IV, laminin and associated proteoglycans with minimal FN[9]. By contrast, FN expression and matrix assembly are upregulated during development, angiogenesis and flow-dependent vessel remodelling[10–12]. FN is also deposited in the intima at athero-prone regions of arteries[13]. This occurs even in athero-resistant wild-type (WT) mice, associated with endothelial inflammatory gene expression, indicating that it is an early event. FN increases in hypercholesterolemic mice together with atherosclerotic plaque progression. Studies in genetically modified mice support a causal role for FN in atherosclerosis[14–16].

In vitro studies with endothelial cells (ECs) showed that disturbed flow or acute changes in flow activate inflammatory pathways such as NF-κB, and induce expression of leukocyte recruitment molecules such as ICAM-1, MCP-1 and VCAM-1[17,18]. However, these events depend strongly on the ECM proteins to which the ECs adhere: cells on collagen I or IV, or basement membrane protein (Matrigel) suppress NF-κB, JNK and PAK in response to flow and soluble inflammatory mediators but are activated in ECs on FN[13,19–21]. Selective activation of cyclic AMP and protein kinase A (PKA) in cells on collagen or basement membrane protein relative to FN mediates the suppression of inflammatory pathways[22,23]. But how different integrins control cAMP/PKA and inflammation is unknown.

The major FN receptor, α5β1, and the major collagen/laminin receptor, α2β1, that are strongly implicated in pro- versus anti-inflammatory signalling *in vitro* and *in vivo*[24,25] share the common β1 subunit. While α2β1 binds best to fibrillar collagens, it also serves as a functionally relevant receptor for collagen IV and laminins[26]. We therefore hypothesized that the cytoplasmic domains of the unique integrin alpha subunits may determine

differential inflammatory signalling. In this study, we examined chimaeric integrin in which the cytoplasmic tail of integrin α5 was replaced by that of α2. Our results show that ECM-dependent differential inflammatory signalling is due to an interaction of the α5 cytoplasmic domain with the cAMP-specific phosphodiesterase PDE4D5, with consequent regulation of PDE4D5 phosphorylation, probably by protein phosphatase 2A (PP2A).

RESULTS

An integrin α5/2 chimaera blocks flow-dependent inflammatory signalling

To examine ECM-specific signalling, we constructed a chimaeric integrin in which the α5 cytoplasmic tail was replaced with the α2 tail (Fig. 1a). When over-expressed in bovine aortic endothelial cells (BAECs) the integrin α5/2 chimaera localized to the cell surface (Supplementary Fig. 1a) and hetero-dimerized with the integrin β1 subunit similarly to WT (Supplementary Fig. 1b). Chimaera-expressing BAECs adhered and spread normally on FN (Supplementary Fig. 1c and Fig. 2d,e), and showed normal FAK activation, FN fibrillogenesis and alignment in laminar flow (Supplementary Fig. 1d–f). We then investigated shear-dependent inflammatory responses. The critical inflammatory transcription factor NF-κB shows transient activation by onset of flow, and sustained activation by oscillatory flow[27,28]. In both cases, the α5/2 chimaera blocked NF-κB activation (Fig. 1b,c) and expression of the NF-κB target gene product ICAM-1 (Fig. 1d). We also noted that the α5/2 chimaera gave higher basal activation of NF-κB and other inflammatory pathways, but this also occurs with normal ECs on collagen or basement membrane protein[13,21]. While this feature has not been further investigated, the combined results demonstrate that the α5/2 chimaera phenocopies cells on basement membranes.

ECM also modulates endothelial responses to soluble inflammatory mediators[19,24]. IL-1β and oxidized LDL are two critical inflammatory mediators in atherosclerosis that also activate NF-κB. IL-1β and oxidized LDL strongly activated NF-κB in control ECs on FN, whereas control cells on Matrigel, or α5/2 chimaera cells on FN were largely resistant (Fig. 1e–g). Previous results showed that selective activation of the cAMP/PKA pathway suppressed NF-κB on collagen IV–laminin basement membranes[22]. Shear stress activated PKA in cells expressing the α5/2 chimaera but not WT α5 on FN (Fig. 1h). Furthermore, blocking PKA with PKI 14-22 amide, a cell-permeable PKA inhibitor, restored NF-κB activity in chimaera-expressing cells (Fig. 1i). Together, these data show that differential PKA activation and subsequent inflammatory responses are mediated by the integrin αtails.

Integrin chimaera knock-in mice

To investigate the role of integrin α tails *in vivo*, we made knock-in mice in which the exon encoding the endogenous integrin α5 cytoplasmic domain was replaced with that of integrin α2 following Cre-mediated recombination (Fig. 2a). Breeding of α5/2-floxed-neo mice with CMV-Cre TG mice resulted in replacement of WT integrin α5 with the α5/2 chimaera (Fig. 2b,c). These mice were viable and able to reproduce. A complete analysis of these mice will be reported elsewhere; in this study, we focused on endothelial phenotype. To confirm functionality, ECs isolated from WT and knock-in mice were plated on FN. The α5/2 cells showed no differences in adhesion or spreading (Fig. 2d,e), confirming normal function.

Endothelial inflammatory activation marked by elevated expression of FN, ICAM-1 and VCAM-1 occurs in regions of disturbed flow in WT C57Bl6 mice[13] and is a strong marker for susceptibility to atherosclerosis[29,30]. Staining for these proteins in the athero-prone inner curvature of the aortic arch was greatly reduced in integrin α5/2 knock-in mice (Fig. 2f). Thus, the integrin α5/2 chimaera suppresses flow-dependent early inflammation *in vivo*.

PGI_2 mediates flow-dependent cAMP/PKA activation

We next addressed how the ECM–integrin interaction modulates flow-dependent cAMP/PKA activation. The pathway by which flow activates cAMP and PKA is unknown; however, flow can induce PGI_2 (prostacyclin) secretion in ECs31, which binds a Gs-coupled receptor to activate adenylate cyclase and induce cAMP production[32], which promotes vasodilation and inhibits thrombosis and inflammation[33]. To test this pathway, human umbilical vein endothelial cells (HUVECs) on Matrigel were subject to flow with or without the cyclooxygenase (COX) inhibitor aspirin to block PGI_2 synthesis, or the PGI_2 receptor antagonist RO1138452 to block PGI_2 signalling. Both of these treatments efficiently inhibited shear stress-dependent PKA activation (Fig. 3a). They also conferred NF-κB activation by flow in cells on Matrigel (Fig. 3b,c), confirming the importance of PKA in suppressing inflammatory pathways. Similarly, in α5/2 chimaera cells on FN, blocking prostacyclin synthesis (with indomethacin) or the PGI_2 receptor inhibited flow-induced PKA activation (Fig. 3d) and conferred NF-κB activation (Fig. 3e,f). Thus, suppression of NF-κB by adhesion of cells to basement membranes is mediated by prostacyclin and its receptor.

Next, to test whether shear stress-dependent PGI_2 secretion is ECM-specific, we analysed the stable prostacyclin metabolite 6-keto-PGF1α, an approach that circumvents the instability of PGI_2. Flow greatly increased 6-keto-PGF1α production, consistent with published data[31,34]. However, 6-keto-PGF1α levels did not differ between FN and Matrigel (Fig. 3g). Thus, prostacyclin production cannot account for the difference in cAMP and PKA activation in cells on different matrices.

PDE4D is required for ECM-specific NF-κB activation

We next considered whether differential cAMP degradation might mediate the observed ECM specificity. Phosphodiesterases (PDEs) are the enzymes that hydrolyse cAMP to reduce or terminate signalling[35,36]. We focused on the PDE4 family, which are abundant in endothelial cells[37–40]. We reasoned that if PDE4 is critical, its inhibition should restore PKA activation in endothelial cells on FN to levels similar to those on collagen or basement membranes. We first tested the PDE4 inhibitor rolipram, which increased shear-dependent PKA activation in cells on FN (Fig. 4a) and abolished flow-dependent NF-κB activation, without affecting NF-κ activity on collagen (Fig. 4b). By contrast, flow-dependent AMPK activation was unaffected by ECM or rolipram (Supplementary Fig. 2a). PDE4 compartmentalization by protein–protein interactions mediates functional specificity in many systems[41]. Among the PDE4 sub-families, both PDE4C and PDE4D were reported in endothelial cells[42]. The PDE4D subfamily has eleven splicing variants; however, we used a panPDE4D antibody and a PDE4D5-specific antibody to show that PDE4D5 is the only isoform detected in HUVEC and BAEC cells (Supplementary Fig. 2b).

We next examined whether PDE4D5 associates with integrins. Immunoprecipitation of endogenous PDE4D5 from HUVECs with two different antibodies brought down α5 but not α2 integrin (Fig. 4c). Immunoprecipitating WT α5 or the α5/2 chimaera showed that this interaction required the α5 cytoplasmic domain (Fig. 4d). To investigate PDE4D function in flow-dependent NF-κB activation, we performed knockdown and reconstitution experiments. PDE4D knockdown almost completely abolished shear stress-dependent NF-κB activation in cells on FN, which was rescued by an short interfering RNA (siRNA)-resistant construct (Fig. 4e). To test whether targeting PDE4D5 to focal adhesion is sufficient for these effects, we fused the focal adhesion targeting domain of FAK to PDE4D5[43]. This construct strongly localized to focal adhesions in cells on Matrigel (Supplementary Fig. 2c) and conferred flow-induced NF-κB activation (Fig. 4f). This construct also reduced shear stress-dependent Creb phosphorylation, confirming suppression of PKA activity.

Direct interaction between the PDE4D5 UCR2 linker and integrin α5

We next mapped the integrin-binding region in PDE4D5 using bacterially expressed and purified fragments of PDE4D5 (Fig. 5a) to pull down integrin α5 from cell lysates. Binding was observed only with the regulatory upstream conserved region 2 (UCR2) with flanking connecting segments (Fig. 5b). Using purified integrin αtail fusion proteins that form coiled coil domain-mediated homodimers[44], only integrin α5 bound the purified PDE4D5 F2 fragment, indicating that the association is direct and specific (Fig. 5c). Examining a series of deletions (Fig. 5d) showed that the carboxy-terminal 13 amino acids from GST-F1-F2 are required for the interaction (Fig. 5e). Among those 13 amino acids, mutation of $K^{292}KKR^{295}$ to either EEEE or AAAA completely blocked, and single amino acid substitutions partially blocked, the interaction (Fig. 5f). Thus, a short, basic sequence in the connecting segment between UCR2 and the catalytic domain is required for binding integrin α5.

To further validate this interaction, cells expressing WT or mutated GFP-PDE4D5 were plated on FN or collagen, then subject to flow for 15 min. In cells on FN, WT PDE4D5 but not PDE4D5 with a mutated α5-binding sequence co-localized with the focal adhesion marker vinculin; co-localization was also lost in cells on collagen (Fig. 5g). Thus, the interaction with α5 specifically recruits PDE4D5 to focal adhesions.

Integrin α5 binding is required for NF-κB activation on FN

To address whether the interaction between integrin α5 and PDE4D5 is required for pro-inflammatory signalling in cells on FN, we reconstituted PDE4D5 knockdown cells with WT or mutant PDE4D5. Whereas the WT PDE4D5 construct recovered NF-κB activation, 4E and 4A mutants were inactive, as was catalytically dead PDE4D5 (D556A) (Fig. 5h). Thus, PDE4D binding to integrin α5 and catalytic activity are required for inflammatory signalling. Together, these results show that recruitment of PDE4D5 to focal adhesions via α5 binding mediates its pro-inflammatory function by suppressing anti-inflammatory PKA activation.

Regulation of PDE4D phosphorylation by integrin α5

We then considered whether localization of PDE4D5 by integrin α5 is the sole determinant of these effects or whether PDE4 catalytic activity is affected. Assaying catalytic activity of purified PDE4D *in vitro* after addition of recombinant integrin α5 tails revealed no changes. PDE4D5 activity is also regulated by phosphorylation; one important site is Ser651, which can be phosphorylated by Erk and suppresses enzymatic activity[45]. Western blotting with an antibody against this site showed that Ser651 phosphorylation increased in cells on collagen compared with FN, independent of fluid shear stress. Further, the reduced phosphorylation on FN was lost in the 4E mutant (Fig. 6a). Cells expressing the chimaeric integrin α5/2 plated on FN also showed high Ser651 PDE4D phosphorylation compared with WT α5 cells (Fig. 6b). These data suggest either that the integrin α5–PDE4D interaction suppresses Ser651 phosphorylation or that integrin α2 activates it. Analysis of cells expressing WT or 4E mutant PDE4D5 were analysed in suspension or after adhesion to FN-coated dishes. Plating on FN triggered Ser651 dephosphorylation in WT PDE4D5 but not the 4E mutant (Fig. 6c). Chimaeric integrin α5/2 also failed to trigger Ser651 dephosphorylation on FN (Fig. 6c). Thus, binding to integrin α5 in cells on FN induces PDE4D5 Ser651 dephosphorylation.

Proteomic analysis revealed PP2A in PDE4D5 immunoprecipitates in ECs on FN (Supplementary Fig. 3a). Co-immunoprecipitation confirmed this interaction in cells on FN but not Matrigel (Supplementary Fig. 3b). Both the PP2A inhibitor okadaic acid (OA) and siRNA against the PP2A catalytic subunit blocked FN-dependent Ser651 dephosphorylation after plating on FN (Supplementary Fig. 3c) and in stable monolayers (Supplementary Fig. 3d,e) without affecting endothelial cell adhesion, spreading or FAK activation on FN (Supplementary Fig. 4a,b). However, these treatments efficiently blocked NF-κB activation by flow and IL1βon FN (Supplementary Fig. 3f,g).

We next addressed whether Ser651 phosphorylation controls ECM-specific NF-κB activation. For ECs on collagen, expression of phospho-resistant S651A mutant in PDE4D knockdown cells increased NF-κB activity (Fig. 6d). Conversely, in cells on FN, rescue of PDE4D5 knock down with phospho-mimetic S651E mutant failed to restore NF-κB activation (Fig. 6e). These results show that control of PDE4D5 phosphorylation on Ser651 by integrins determines subsequent inflammatory signalling.

Endothelial-specific knockdown of PDE4D inhibits inflammation

We next investigated whether PDE4D is required for flow-dependent inflammatory activation of the endothelium *in vivo* using siRNA. For these experiments, we used recently developed nanoparticles that are highly specific to ECs and do not knock down genes in haematopoietic cells, including leukocytes, or in hepatocytes, even at a high dose (2.0 mg kg^{-1})[46]. We first screened multiple siRNAs and identified a sequence that depleted mouse PDE4D *in vitro* with an IC_{50} of 0.05 nM (Supplementary Fig. 5a), which is ~100× lower than most siRNAs. Transfection into cultured mouse ECs abolished flow-dependent NF-κB activation and ICAM-1 induction, which was rescued by viral expression of human PDE4D5 (Fig. 7a), thus, confirming the efficacy and specificity of this siRNA sequence. A version of this siRNA was chemically modified to improve stability and packaged into nanoparticles,

then injected intravenously into mice (1.0 mg kg^{-1}). Isolation of aortic endothelial messenger RNA 14 days after injection showed a ~70% decrease in PDE4D mRNA compared with the luciferase control siRNA (Supplementary Fig. 5b). C57BL6 mice were then injected three times in a month with PDE4D or luciferase siRNA nanoparticles. The PDE4D siRNA greatly reduced inflammatory gene expression in an athero-prone artery segment compared with luciferase siRNA (Fig. 7b).

Effects on atherosclerosis

Lastly, we investigated atherosclerosis in the integrin α5/2 chi-maeric mice by breeding onto the hypercholesterolemic ApoE$^{-/-}$background, which, on a high-fat, 'Western' diet, develop atherosclerotic plaques at regions of disturbed flow, similar to human disease[47]. Aortae from these mice after 4 months on a high-fat diet showed dramatically decreased plaque burden (Fig. 7c). These results validate the connection between early inflammatory activation of the endothelium by disturbed shear and later disease progression in hyperlipidaemia.

DISCUSSION

Inflammation has frequently been described as a double-edged sword that is required for tissue defence, remodelling and repair but, if not properly regulated, causes damage or disease[48,49]. Inflammatory reactions therefore need to be initiated following infection, injury or stress, but then resolved when the infection is cured, injury healed or stress relieved. Linking the biochemical and structural changes associated with tissue repair and remodelling with the pathways that govern inflammation appears to be essential for proper regulation of these processes[50,51].

Vascular remodelling to adapt to changes in tissue demand requires inflammatory activation of the endothelium and recruitment of leukocytes, mainly monocytes, which aid in remodelling[6,7]. These processes also involve degradation of basement membranes and synthesis of a provisional, FN-rich ECM. Once morphogenesis is completed, new basement membrane synthesis is a key part of the resolution phase for formation of stable, quiescent vessels[52,53]. Atherosclerosis may be considered a form of pathological flow-dependent remodelling where ECs in regions of disturbed flow undergo inflammatory activation but can never adapt to restore quiescence[54]. WT mice show chronic inflammatory activation of the endothelium in regions of disturbed flow[55] that, when other risk factors are present, progresses to atherosclerosis. FN deposition beneath the endothelium is an early event in this process, appearing first in the regions of low-grade inflammation in WT mice and increasing in atherosclerosis[13]. FN in the endothelial layer is also abundant in lesions from human arteries[56]. Moreover, several genetic manipulations that reduce FN in the vessel wall reduce atherosclerosis in mice[14–16], as does an antagonist of integrin α5β1 (ref. 24). Interestingly, while classic genetic studies that searched for single genes that affect artery disease identified mainly lipid metabolism and inflammatory genes, a recent analysis of gene networks identified ECM and ECM remodelling gene networks as equivalently important[57]. Thus, genetic analysis supports a role for tight integration of inflammatory and ECM pathways in vascular remodelling.

Previous work showed that in cells on collagen or basement membrane, flow-induced activation of the cAMP/PKA pathway inhibits inflammatory activation of the endothelium[22]. Recent work has also identified PKA-independent anti-inflammatory actions of cAMP on inflammasome assembly[58–60]. The provisional FN-rich ECM relieves this inhibition and allows inflammatory activation. Our data show that these effects are mediated through direct binding of PDE4D5 to the integrin α5 tail. This interaction localizes PDE4D5 to focal adhesions, induces its proximity to PP2A, with subsequent dephosphorylation on an inhibitory site. This dephosphorylation increases enzymatic activity to decrease cAMP levels and increase endothelial inflammatory activation. These effects were observed both *in vitro* and *in vivo*, the latter in mice where the integrin α5 cytoplasmic domain was replaced with that of α2, and after knockdown of PDE4D5.

Ser651 of PDE4D5 is potentially phosphorylated by Erk2 (ref. 45). However, in cells on collagen or basement membrane, Ser651 phosphorylation was high in both high and low serum, and was unaffected by the MEK inhibitor U0126 despite large changes in Erk activity, and was adhesion-independent. Instead, PDE4D5 Ser651 phosphorylation was controlled by matrix-specific, PP2A-dependent dephosphorylation. Thus, plating cells on FN or shear stress-dependent integrin activation results in recruitment of PDE4D5 into focal adhesions and dephosphorylation of Ser651.

A number of anti-inflammation drugs are in development or clinical trial for treatment of atherosclerosis[61]. Interestingly, both genetic deletion of plasma FN and an integrin α5β1 antagonist reduced atherosclerotic plaque development in mouse models[16,23]. However, FN contributes to haemostasis, fibrosis and other essential functions; thus, its systemic inhibition is unlikely to be clinically viable[62,63]. The integrin α5–PDE4D interaction may therefore provide a more specific target to inhibit plaque progression without globally affecting FN function. It should also bypass adverse effects of PDE4 catalytic inhibitors[35]. Further studies will be required to understand how the molecular events and interactions defined here play out during the complex physiology and pathology of vessel remodelling, atherosclerosis and other instances of chronic inflammation.

METHODS

Cell culture

BAECs were grown in DMEM containing 10% FBS and penicillin/streptomycin. HUVECs were grown in DMEM/F12, 10% FBS, 5 mg ml^{-1} ECGS, 100 μg ml^{-1} heparin, penicillin/streptomycin or EGM media (Lonza). Mouse endothelial cells were grown in DMEM containing 20% FBS, 1× non-essential amino acids (Gibco), 2 mM L-glutamate, 50 μg ml^{-1} gentamicin, 4 μg ml^{-1} amphotericin B, 100 μg ml^{-1} heparin, 5 mg ml^{-1} ECGS and penicillin/streptomycin. Primary mouse endothelial cells were isolated from the lung, using rat anti-mouse CD31 antibody (clone MEC13.3, Pharmingen, no. 553370) and Dynabeads (cat. no. 110.35, Invitrogen) as previously described[64]. No cell lines were used in this study.

Generation of BAECs expressing the integrin α5/2 chimaera

BAECs were infected with retrovirus containing human wild-type (WT) integrin α5 or the α5/2 chimaera. Infected cells were selected with puromycin (0.5 μg ml^{-1}) and FACS-sorted for high expressors with mAb16, which recognizes human-specific integrin α5 extracellular domain. Similar surface expression of WT and integrin chimaera was achieved by sorting.

Generation of immortalized mouse aortic endothelial cells expressing NF-κB reporter

Immortalized mouse aortic endothelial cells were first infected with lentivirus containing human PDE4D5-GFP and sorted for the cells with similar level of expression to endogenous PDE4D5. The cells were then infected with lentivirus for NF-κB reporter[65], which induces expression of GFP following NF-κB activation.

Plasmids and siRNA

Human integrin α5 WT and integrin α5/2 chimaera were cloned into pLPCX (Clontech) using NotI and ClaI sites. The α2 tail sequence was fused to the α5 sequence in frame by PCR using primers containing α2 tail sequences. siRNA-resistant PDE4D5 WT and mutants were first cloned into pBOB-GFP vector using XbaI and AgeI sites. Then PDE4D5-GFP fragments were PCR-amplified using the primers, 5′-gcaagcttatggctcagcagacaagcccgg-3′ and 5′-gaattctta cttgtacagctcgtccatgc-3′, and then subcloned into pLPCX vector using HindIII and EcoRI sites. For introducing silent mutations into human PDE4D5, the sequence 5′-atacaaactctgagttggccttgatgta-3′ was used. The PDE4D siRNA sequence used in cultured cells was 5′-AAGAACUUGCCUUGAUGUACA-3′ from ref. 66. The siRNA for *in vivo* knockdown of PDE4D was 5′-GAACGAGAUUUGUUAAAA AdTdT-3′, and the siRNA for *in vivo* knockdown of luciferase was 5′-CUUACG CUGAGUACUUCGAdTdT-3′ (ref. 46). siRNAs used *in vivo* were modified to prevent immunostimulation, as previously described[46,67]. PDE4D5 F2, F3 and F4 fragments cloned into pGEX-4T1 were previously described[66]. The other PDE4D5 fragments were PCR-amplified and cloned into pGEX-4T1 vector between EcoRI and XhoI sites. For deletion fragment analysis used in Fig. 5e, the following amino acid sequences of PDE4D5 were fused to GST; Δ1:123–284, Δ2: 123–272, Δ3: 123–260, Δ4: 123–248. Two siRNA sequences for bovine PP2A-Cα are 5′-CCAU GACCGAAAUGUAGUAdTdT-3′ and 5′-GCAUGACUGUAGAUAAGAAdTd T-3′. FAT-PDE4D5-GFP was constructed by inserting FAT domain (cloned from HUVEC cDNA) into the amino terminus of the pLPCX-PDE4D5-GFP construct using Gibson assembly.

Animals

The integrin α5/2 chimaera C57BL/6 strain was generated using homologous recombination by OZgene (Australia). Floxed-Neo mice were crossed with the CMV-Cre line (stock number 006054) to create the chimaera knock-in mice. For atherosclerosis analysis, integrin chimaera knock-in mice were bred with ApoE null mice (stock number 002052). All animal experiments were performed under protocols approved by Yale University Institutional Animal Care and Use. No statistical method was used to predetermine sample size. The animal experiments were not randomized. The investigators were not blinded to allocation during experiments and outcome assessment.

Shear stress experiments

Serum-starved endothelial cells were replated on glass slides coated with the indicated proteins for 5 h before flow application. The slides were loaded into parallel plate flow chambers. Pulsatile laminar shear of 15 ± 5 dynes cm^{-2} was used to mimic flow profile in athero-resistant regions of artery. Oscillatory shear of 1 ± 5 dynes cm^{-2}, 1 Hz was used to mimic disturbed flow in athero-prone regions.

Measurement of prostacyclin production

To measure the stable prostacyclin metabolite 6-keto-PGF1α, HUVECs were starved overnight in 1% medium containing 1% FBS, and then were plated on glass slides coated with FN or Matrigel for 5 h to form a confluent monolayer. Cells were then treated with pulsatile laminar shear (15 ± 5 dynes cm^{-2}) for 90 min or left untreated. The medium was centrifuged to remove detached cells and 6-keto-PGF1α assayed using the ELISA kit (Enzo life sciences) according to the manufacturer's instructions.

In vivo PDE4D knockdown

PDE4D siRNA or control luciferase siRNA was packaged into endothelial-specific nanoparticles and injected at 1 mg kg^{-1} via tail vein into WT (C57Bl6) mice. After two weeks, mouse aortae were isolated and intimal RNA was prepared as described previously[68]. Briefly, mice were euthanized according to the Yale University IACUC protocol. Aortae were isolated and flushed with 250 μl QIAzol lysis reagent by insulin syringe to elute endothelial RNA, which was purified by miRNeasy mini kit (Qiagen) and amplified using a whole transcriptome amplification kit (Qiagen) according to the manufacturer's instructions. PDE4D transcript levels were measured by qRT-PCR using amplified diluted cDNA template. After confirming the dose and time course for *in vivo* PDE4D knockdown, WT (C57Bl6) mice were injected with PDE4D or control siRNA, once a week for 3 weeks. Aortae were harvested at the end of the fourth week and stained for inflammatory markers. Four male mice (3 month old) were used for each condition.

Immunohistochemistry

Mice were euthanized according to the Yale University IACUC protocol and perfused via the left ventricle with 4% paraformaldehyde (PFA). Aortae along with carotid branches were dissected and fixed overnight in PFA. For cryosections, tissue was embedded in OCT and frozen on dry ice. Longitudinal cryosections (10–15 μm) were prepared with the cryostat. For immunostaining, cryosections were fixed in −20 °C acetone for 10 min. Sections were blocked in IHC-Tek antibody diluent for 1 h at room temperature, and were then incubated with primary antibodies at the indicated concentrations in IHC-Tek antibody diluent overnight at 4 °C. After washing 3 times in PBS, sections were incubated with Alexa Flour 598-conjugated Donkey anti rabbit/rat secondary antibody (1:200, Invitrogen) for 1 h at room temperature. After washing with PBS, sections were mounted in Vectashield with DAPI (Vector Laboratories) and images taken using a confocal microscope. Four male mice (3 month old) were used for each condition to monitor inflammatory markers on the inner curvature of the aortic arch. For atherosclerosis analysis, the integrin chimaera mice in ApoE

null background (4 male mice with age of three months) were on high-fat diet for 4 months. Aortae were opened and stained en face with Sudan IV.

Antibodies

Anti-p-NF-κB p65 (Ser536): rabbit monoclonal antibody (93H1), Cell Signaling (3033L), 1:1,000 for immunoblotting; anti-p-Creb (Ser133): rabbit monoclonal antibody (87G3), Cell Signaling (9198S), 1:1,000 for immunoblot-ting; anti-PKAc: mouse monoclonal antibody, BD Transduction Laboratories (610981), 1:1,000 for immunoblotting; anti-integrin α2: rabbit polyclonal, Millipore (AB1936), 1:1,000 for immunoblotting; anti-VCAM-1: rabbit monoclonal antibody (EPR5047), Abcam (ab134047), 1:200 for immunohistochemistry; anti-ICAM-1: rat monoclonal antibody (YN1/1.7.4.), BioLegend (116101), 1:200 for immunohistochemistry; anti-ICAM-1: rabbit polyclonal, Abcam (ab124759), 1:1,000 for immunoblotting; anti-NF-κB-p65: rabbit polyclonal (C-20), Santa Cruz (sc-372), 1:2,000 for immunoblotting; anti-vinculin: mouse monoclonal antibody (VIN-11-5), Sigma (V4505), 1:500 for immunohistochemistry; anti-fibronectin: rabbit polyclonal, Sigma (F3648), 1:400 for immunohistochemistry; anti-p-FAK (Tyr397): rabbit polyclonal, Cell Signaling (3283S), 1:1,000 for immunoblotting; anti-FAK: rabbit polyclonal, Cell Signaling (3285S), 1:1,000 for immunoblotting; anti-PP2A, C subunit: mouse monoclonal antibody (1D6), Millipore (05-421), 1:1,000 for immunoblotting.

Band intensities from immunoblotting were quantified by densitometry using ImageJ software.

PKA activity assay

Active PKA was isolated by pulldowns with GST-PKI and quantified as described previously[69]. In brief, bacterially expressed GST-PKI was immobilized on GSH-agarose beads. Cell lysates were prepared in lysis buffer containing 25 mM Tris-HCl, pH 7.4, 0.5 mM EDTA, 0.5 mM EGTA, 10 mM β-mercaptoethanol, protease inhibitor cocktail and 1 mM phenylmethylsulfonyl fluoride. After brief sonication and centrifugation, the supernatants were added with 100 μM ATP and 1 mM $MgCl_2$, then incubated with the GST-PKI beads for 20 min at 4°C and washed three times with wash buffer (50 mM Tris, pH 7.4, 100 μM ATP and 1 mM $MgCl_2$). Bound active PKA was eluted with sample buffer and immunoblotted with anti-PKA catalytic subunit antibody (BD).

Immunoprecipitation

Cells were lysed in 20 mM PIPES pH 6.8, 1% TX-100, 150 mM NaCl, 150 mM sucrose, 0.2% sodium deoxycholate, 500 μM EDTA and protease inhibitors. After incubation on ice for 15 min and centrifugation, supernatants were diluted 10× in buffer containing 20 mM PIPES pH 6.8, 1% TX-100, 150 mM NaCl, 150 mM sucrose, 2.5 mM $MgCl_2$ and 2.5 mM $MnCl_2$. Antibody-conjugated protein A beads were incubated with the lysates for 2 h at 4 °C before washing with dilution buffer.

Proteomic analysis for PDE4D5 binding proteins

FLAG-tagged PDE4D5 was stably expressed in BAECs using retroviral infection. The cells were plated on FN for 30 min and lysed for immunoprecipitation with FLAG antibody.

FLAG peptides were used to elute from immune complexes from control non-infected cells and PDE4D5-expressing cells. After SDS–PAGE and silver staining, specific bands were excised and submitted to Yale Keck Biotechnology Resource Laboratory for LC–MS/MS analysis.

In vitro binding assays

For the binding assay using integrin tails on beads, 30 μg of integrin αtail proteins were incubated with 6 μl of cobalt beads (Clontech). Washed beads were incubated with 100 ng of purified PDE4D5 fragment for 1 h in buffer containing 20 mM PIPES pH 6.8, 1% TX-100, 150 mM NaCl, 150 mM sucrose. For GST-pulldown analysis for PDE4D domain mapping, 5 μg of GST fusion proteins on GSH-agarose beads were incubated with 100 ng of purified integrin α5 tail proteins in buffer containing 20 mM PIPES pH 6.8, 1% TX-100, 150 mM NaCl, 150 mM sucrose and 1 mg ml^{-1} BSA for 1 h at 4 °C, then washed and analysed by SDS–PAGE and western blotting.

Cell adhesion and spreading assay

Cells were detached and replated on dishes coated with either poly-L-lysine or FN (10 μg ml^{-1}) for 15 min. Adherent cells were quantified using the acid phosphatase assay[70] and normalized to the cells attached on PLL-coated dishes for 1 h. To assess cell spreading, cells plated for the indicated times were fixed and stained with Alexa Fluor 488-conjugated wheat germ agglutinin (Invitrogen, 5 μg ml^{-1}), imaged with spinning-disc confocal microscopy (Nikon) and cell areas were quantified using ImageJ software.

Fibronectin fibrillogenesis assay

WT or α5/2 cells were plated on FN-coated coverslips and grown until they formed monolayers. Cells were incubated with 1 % FBS containing media for three days, fixed and then stained with anti-FN antibody (Sigma).

Statistics and reproducibility

Statistics were analysed using Student's *t*-test or one-way ANOVA (multiple comparisons) in GraphPad Prism 6. Statistical significance was taken as $P < 0.05$. Data are represented as means ± s.e.m. Pulldown and co-immunoprecipitation results were confirmed in three independent experiments.

Data availability

Statistics source data are available in Supplementary Table 1. All other data are available from the authors on request.

Supplementary Material

Refer to Web version on PubMed Central for supplementary material.

Acknowledgments

We thank K. Yamada (NIH, USA), D. Calderwood (Yale University, USA), H. Kim (POSTECH, Korea) and A. Jayaraman (Texas A&M University, USA) for providing reagents, and J. Hwa (Yale University, USA) for advice on

prostacyclin experiments. Lipid analysis was done by the Yale Mouse Phenotypic Center, supported by a U24 DK059635 grant. This work was funded by a National Institutes of Health grant 5R01HL75092 to M.A.S. G.B. is funded by an MRC project grant (MR/J007412/1). We are grateful to R. Webber and N. Copeland for maintaining the mouse colonies used in this study.

References

1. Galkina E, Ley K. Immune and inflammatory mechanisms of atherosclerosis. Annu Rev Immunol. 2009; 27:165–197. [PubMed: 19302038]
2. Zarins CK, et al. Carotid bifurcation atherosclerosis. Quantitative correlation of plaque localization with flow velocity profiles and wall shear stress. Circ Res. 1983; 53:502–514. [PubMed: 6627609]
3. Caro CG, Fitz-Gerald JM, Schroter RC. Arterial wall shear and distribution of early atheroma in man. Nature. 1969; 223:1159–1161. [PubMed: 5810692]
4. Libby P, Ridker PM, Hansson GK. Progress and challenges in translating the biology of atherosclerosis. Nature. 2011; 473:317–325. [PubMed: 21593864]
5. Conway DE, Schwartz MA. Flow-dependent cellular mechanotransduction in atherosclerosis. J Cell Sci. 2013; 126:5101–5109. [PubMed: 24190880]
6. Gaudet AD, Popovich PG. Extracellular matrix regulation of inflammation in the healthy and injured spinal cord. Exp Neurol. 2014; 258:24–34. [PubMed: 25017885]
7. Bollyky P, Bogdani M, Bollyky J, Hull R, Wight T. The role of hyaluronan and the extracellular matrix in islet inflammation and immune regulation. Curr Diab Rep. 2012; 12:471–480. [PubMed: 22810951]
8. Papageorgiou AP, Heymans S. Interactions between the extracellular matrix and inflammation during viral myocarditis. Immunobiology. 2012; 217:503–510. [PubMed: 21907443]
9. Grant DS, Kleinman HK, Martin GR. The role of basement membranes in vascular development. Ann NY Acad Sci. 1990; 588:61–72. [PubMed: 2192650]
10. Kim S, Bell K, Mousa SA, Varner JA. Regulation of angiogenesis *in vivo* by ligation of integrin α5β1 with the central cell-binding domain of fibronectin. Am J Pathol. 2000; 156:1345–1362. [PubMed: 10751360]
11. Chiang HY, Korshunov VA, Serour A, Shi F, Sottile J. Fibronectin is an important regulator of flow-induced vascular remodeling. Arterioscler Thromb. 2009; 29:1074–1079.
12. Chiu CH, Chou CW, Takada S, Liu YW. Development and fibronectin signaling requirements of the zebrafish interrenal vessel. PLoS ONE. 2012; 7:e43040. [PubMed: 22937010]
13. Orr AW, et al. The subendothelial extracellular matrix modulates NF-κB activation by flow: a potential role in atherosclerosis. J Cell Biol. 2005; 169:191–202. [PubMed: 15809308]
14. Tan MH, et al. Deletion of the alternatively spliced fibronectin EIIIA domain in mice reduces atherosclerosis. Blood. 2004; 104:11–18. [PubMed: 14976060]
15. Babaev VR, et al. Absence of regulated splicing of fibronectin EDA exon reduces atherosclerosis in mice. Atherosclerosis. 197:534–540.
16. Rohwedder I, et al. Plasma fibronectin deficiency impedes atherosclerosis progression and fibrous cap formation. EMBO Mol Med. 2012; 4:564–576. [PubMed: 22514136]
17. Nagel T, Resnick N, Atkinson WJ, Dewey CF Jr, Gimbrone MA Jr. Shear stress selectively upregulates intercellular adhesion molecule-1 expression in cultured human vascular endothelial cells. J Clin Invest. 1994; 94:885–891. [PubMed: 7518844]
18. Bao X, Lu C, Frangos JA. Temporal gradient in shear but not steady shear stress induces PDGF-A and MCP-1 expression in endothelial cells: role of NO, NFκB, and egr-1. Arterioscler Thromb. 1999; 19:996–1003.
19. Orr AW, et al. Matrix-specific p21-activated kinase activation regulates vascular permeability in atherogenesis. J Cell Biol. 2007; 176:719–727. [PubMed: 17312022]
20. Orr AW, Hahn C, Blackman BR, Schwartz M. A p21-activated kinase signaling regulates oxidant-dependent NF-κB activation by flow. Circ Res. 2008; 103:671–679. [PubMed: 18669917]
21. Hahn C, Orr AW, Sanders JM, Jhaveri KA, Schwartz MA. The subendothelial extracellular matrix modulates JNK activation by flow. Circ Res. 2009; 104:995–1003. [PubMed: 19286608]

22. Funk SD, et al. Matrix-specific protein kinase a signaling regulates p21-activated kinase activation by flow in endothelial cells. Circ Res. 2010; 106:1394–1403. [PubMed: 20224042]
23. Yurdagul A, et al. Altered nitric oxide production mediates matrix-specific PAK2 and NF-κB activation by flow. Mol Biol Cell. 2013; 24:398–408. [PubMed: 23171552]
24. Yurdagul A, et al. α5β1 integrin signaling mediates oxidized low-density lipoprotein-induced inflammation and early atherosclerosis. Arterioscler Thromb. 2014; 34:1362–1373.
25. Orr AW, Ginsberg MH, Shattil SJ, Deckmyn H, Schwartz MA. Matrix-specific suppression of integrin activation in shear stress signaling. Mol Biol Cell. 2006; 17:4686–4697. [PubMed: 16928957]
26. Madamanchi, A., Santoro, SA., Zutter, MM. I Domain Integrins. Gullberg, D., editor. Springer; 2014. p. 41-60.
27. Wang C, Baker BM, Chen CS, Schwartz MA. Endothelial cell sensing of flow direction. Arterioscler Thromb. 2013; 33:2130–2136.
28. Khachigian LM, Resnick N, Gimbrone MA Jr, Collins T. Nuclear factor-kappa B interacts functionally with the platelet-derived growth factor B-chain shear-stress response element in vascular endothelial cells exposed to fluid shear stress. J Clin Invest. 1995; 96:1169–1175. [PubMed: 7635955]
29. Glagov S, Zarins C, Giddens D, Ku DN. Hemodynamics and atherosclerosis. Insights and perspectives gained from studies of human arteries. Arch Pathol Lab Med. 1988; 112:1018–1031. [PubMed: 3052352]
30. Frangos SG, Gahtan V, Sumpio B. Localization of atherosclerosis: role of hemodynamics. Arch Surg. 1999; 134:1142–1149. [PubMed: 10522862]
31. Frangos JA, Eskin SG, McIntire LV, Ives CL. Flow effects on prostacyclin production by cultured human endothelial cells. Science. 1985; 227:1477–1479. [PubMed: 3883488]
32. Fetalvero KM, Martin KA, Hwa J. Cardioprotective prostacyclin signaling in vascular smooth muscle. Prostaglandins Other Lipid Mediat. 2007; 82:109–118. [PubMed: 17164138]
33. Stitham J, Midgett C, Martin K, Hwa J. Prostacyclin: an inflammatory paradox. Front Pharmacol. 2011; 2:24. [PubMed: 21687516]
34. Tsai MC, et al. Shear stress induces synthetic-to-contractile phenotypic modulation in smooth muscle cells via peroxisome proliferator-activated receptor α/δ activations by prostacyclin released by sheared endothelial cells. Circ Res. 2009; 105:471–480. [PubMed: 19628794]
35. Maurice DH, et al. Advances in targeting cyclic nucleotide phosphodiesterases. Nat Rev Drug Discov. 2014; 13:290–314. [PubMed: 24687066]
36. Baillie GS. Compartmentalized signalling: spatial regulation of cAMP by the action of compartmentalized phosphodiesterases. FEBS J. 2009; 276:1790–1799. [PubMed: 19243430]
37. Muzaffar S, Jeremy JY, Angelini GD, Shukla N. NADPH oxidase 4 mediates upregulation of type 4 phosphodiesterases in human endothelial cells. J Cell Physiol. 2012; 227:1941–1950. [PubMed: 21732365]
38. Wang J, Bingaman S, Huxley VH. Intrinsic sex-specific differences in microvascular endothelial cell phosphodiesterases. Am J Physiol Heart Circ Physiol. 2010; 298:H1146–H1154. [PubMed: 20139324]
39. Netherton SJ, Maurice DH. Vascular endothelial cell cyclic nucleotide phosphodiesterases and regulated cell migration: implications in angiogenesis. Mol Pharmacol. 2005; 67:263–272. [PubMed: 15475573]
40. Thompson WJ, et al. Regulation of cyclic AMP in rat pulmonary microvascular endothelial cells by rolipram-sensitive cyclic AMP phosphodiesterase (PDE4). Biochem Pharmacol. 2002; 63:797–807. [PubMed: 11992650]
41. McCormick K, Baillie GS. Compartmentalisation of second messenger signalling pathways. Curr Opin Genet Dev. 2014; 27:20–25. [PubMed: 24791689]
42. Pullamsetti SS, et al. cAMP phosphodiesterase inhibitors increases nitric oxide production by modulating dimethylarginine dimethylaminohydrolases. Circulation. 2011; 123:1194–1204. [PubMed: 21382892]

43. Hildebrand JD, Schaller MD, Parsons JT. Identification of sequences required for the efficient localization of the focal adhesion kinase, pp125FAK, to cellular focal adhesions. J Cell Biol. 1993; 123:993–1005. [PubMed: 8227154]
44. Pfaff M, Liu S, Erle DJ, Ginsberg MH. Integrin β cytoplasmic domains differentially bind to cytoskeletal proteins. J Biol Chem. 1998; 273:6104–6109. [PubMed: 9497328]
45. MacKenzie SJ, Baillie GS, McPhee I, Bolger GB, Houslay MD. ERK2 mitogen-activated protein kinase binding, phosphorylation, and regulation of the PDE4D cAMP-specific phosphodiesterases: The involvement of COOH-terminal docking sites and NH2-terminal UCR regions. J Biol Chem. 2000; 275:16609–16617. [PubMed: 10828059]
46. Dahlman JE, et al. In vivo endothelial siRNA delivery using polymeric nanoparticles with low molecular weight. Nat Nanotech. 2014; 9:648–655.
47. Plump AS, et al. Severe hypercholesterolemia and atherosclerosis in apolipoprotein E-deficient mice created by homologous recombination in ES cells. Cell. 1992; 71:343–353. [PubMed: 1423598]
48. Smith JA. Neutrophils, host defense, and inflammation: a double-edged sword. J Leukoc Biol. 1994; 56:672–686. [PubMed: 7996043]
49. Morganti-Kossmann MC, Rancan M, Stahel PF, Kossmann T. Inflammatory response in acute traumatic brain injury: a double-edged sword. Curr Opin Crit Care. 2002; 8:101–105. [PubMed: 12386508]
50. Arroyo AG, Iruela-Arispe ML. Extracellular matrix, inflammation, and the angiogenic response. Cardiovasc Res. 2010; 86:226–235. [PubMed: 20154066]
51. Sorokin L. The impact of the extracellular matrix on inflammation. Nat Rev Immunol. 2010; 10:712–723. [PubMed: 20865019]
52. Stratman AN, Malotte KM, Mahan RD, Davis MJ, Davis GE. Pericyte recruitment during vasculogenic tube assembly stimulates endothelial basement membrane matrix formation. Blood. 2009; 114:5091–5101. [PubMed: 19822899]
53. Davis GE, Senger DR. Endothelial extracellular matrix: biosynthesis, remodeling, and functions during vascular morphogenesis and neovessel stabilization. Circ Res. 2005; 97:1093–1107. [PubMed: 16306453]
54. Hahn C, Schwartz MA. The role of cellular adaptation to mechanical forces in atherosclerosis. Arterioscler Thromb. 2008; 28:2101–2107.
55. Jongstra-Bilen J, et al. Low-grade chronic inflammation in regions of the normal mouse arterial intima predisposed to atherosclerosis. J Exp Med. 2006; 203:2073–2083. [PubMed: 16894012]
56. Kakolyris S, Karakitsos P, Tzardi M, Agapitos E. Immunohistochemical detection of fibronectin in early and advanced atherosclerosis. In Vivo. 1995; 9:35–40. [PubMed: 7669946]
57. Ghosh S, et al. Systems genetics analysis of genome-wide association study reveals novel associations between key biological processes and coronary artery disease. Arterioscler Thromb. 2015; 35:1712–1722.
58. Lee GS, et al. The calcium-sensing receptor regulates the NLRP3 inflammasome through Ca^{2+} and cAMP. Nature. 2012; 492:123–127. [PubMed: 23143333]
59. Sokolowska M, et al. Prostaglandin E2 inhibits NLRP3 inflammasome activation through EP4 receptor and intracellular cyclic AMP in human macrophages. J Immunol. 2015; 194:5472–5487. [PubMed: 25917098]
60. Yan Y, et al. Dopamine controls systemic inflammation through inhibition of NLRP3 inflammasome. Cell. 2015; 160:62–73. [PubMed: 25594175]
61. Libby P, Okamoto Y, Rocha VZ, Folco E. Inflammation in atherosclerosis transition from theory to practice. Circ J. 2010; 74:213–220. [PubMed: 20065609]
62. Ni H, et al. Plasma fibronectin promotes thrombus growth and stability in injured arterioles. Proc Natl Acad Sci USA. 2003; 100:2415–2419. [PubMed: 12606706]
63. Sakai T, et al. Plasma fibronectin supports neuronal survival and reduces brain injury following transient focal cerebral ischemia but is not essential for skin-wound healing and hemostasis. Nat Med. 2001; 7:324–330. [PubMed: 11231631]

64. Allport JR, et al. Neutrophils from MMP-9- or neutrophil elastase-deficient mice show no defect in transendothelial migration under flow *in vitro*. J Leukoc Biol. 2002; 71:821–828. [PubMed: 11994507]

65. Tian J, Alimperti S, Lei P, Andreadis ST. Lentiviral microarrays for real-time monitoring of gene expression dynamics. Lab Chip. 2010; 10:1967–1975. [PubMed: 20520864]

66. Kim HW, et al. Cyclic AMP controls mTOR through regulation of the dynamic interaction between Rheb and phosphodiesterase 4D. Mol Cell Biol. 2010; 30:5406–5420. [PubMed: 20837708]

67. Love KT, et al. Lipid-like materials for low-dose, *in vivo* gene silencing. Proc Natl Acad Sci USA. 2010; 107:1864–1869. [PubMed: 20080679]

68. Nam D, et al. Partial carotid ligation is a model of acutely induced disturbed flow, leading to rapid endothelial dysfunction and atherosclerosis. Am J Physiol Heart Circ Physiol. 2009; 297:H1535–H1543. [PubMed: 19684185]

69. Paulucci-Holthauzen AA, O'Connor KL. Use of pseudosubstrate affinity to measure active protein kinase A. Anal Biochem. 2006; 355:175–182. [PubMed: 16842735]

70. Yang TT, Sinai P, Kain SR. An acid phosphatase assay for quantifying the growth of adherent and nonadherent cells. Anal Biochem. 1996; 241:103–108. [PubMed: 8921171]

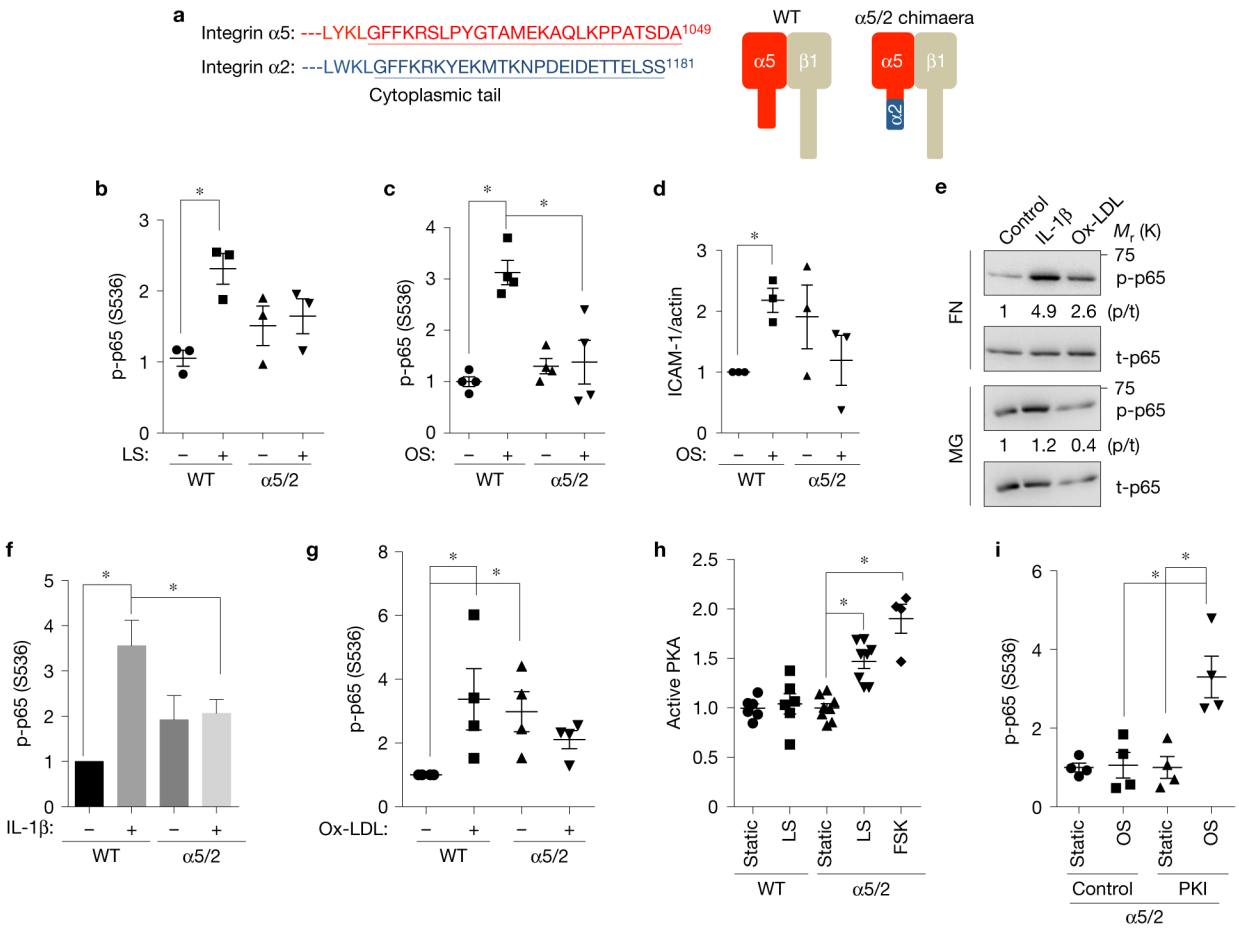

Figure 1.

Integrin α subunit cytoplasmic tails determine ECM-specific inflammatory signalling. (**a**) Alignment of integrin α subunit tail sequences and schematic representation of integrin α5/2 chimaera. (**b**,**c**) NF-κB activation by flow. WT α5 or α5/2 cells on FN (20 μg ml^{-1}) were subjected to 30 min laminar shear (**b**) or 18 h oscillatory shear (**c**). NF-κB activation was then assayed by western blotting for Ser536 p65 phosphorylation (**b**, $n = 3$; **c**, $n = 4$). *Y* axis values throughout the figure represent the fold change (relative to control). LS, laminar shear; OS, oscillatory shear. (**d**) Induction of ICAM-1 after 18 h of oscillatory flow in cells expressing WT α5 versus the α5/2 chimaera on FN ($n = 3$). (**e**–**g**) NF-κB activation by soluble atherogenic factors. WT BAECs on FN or diluted Matrigel (MG) were stimulated with IL-1β or oxidized LDL for 30 min. NF-κB was assayed by western blotting for pSer536 p65 (**e**). t-p65, total p65. Quantification in **f** ($n = 7$) and **g** ($n = 4$) shows activation relative to control cells on FN without flow. (**h**) Effect of the chimaera on PKA activation. WT α5 or α5/2 chimaera cells on FN were sheared for 15 min and active PKA was pulled down from cell lysates with GST-PKI followed by immunoblotting. Forskolin (FSK) was used as a positive control for PKA activation (n= 4–8). (**i**) PKA inhibition rescues NF-κB activation in α5/2 chimaera cells. Chimaera cells on FN were treated with the PKI 14–22 amide inhibitor or dimethylsulfoxide (DMSO) alone, and then subjected to oscillatory shear for 18 h. Activation of NF-κB was assayed by western blotting (n= 4). Data are represented

as means ± s.e.m. $^{*}P < 0.05$ by one-way ANOVA (**b**,**c**,**h**,**i**) or two-tailed *t*-test (**d**,**f**,**g**). In all panels *n* values represent independent experiments. Source data are provided in Supplementary Table 1. Unprocessed scans of blots are shown in Supplementary Fig. 6.

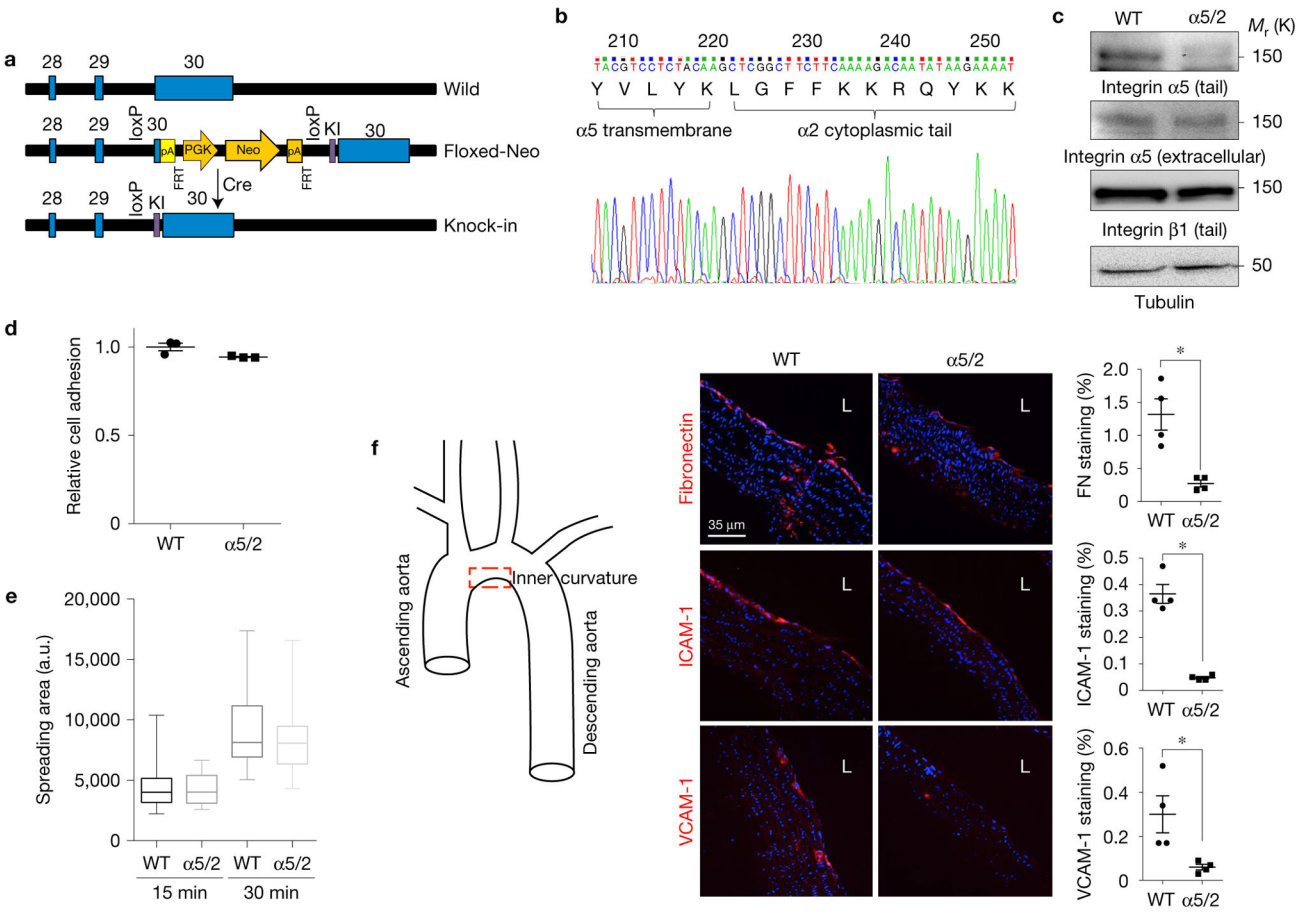

Figure 2.

Integrin chimaera knock-in mouse showed reduced inflammation in artery. (**a**) Targeting strategy. These floxed, knock-in mice were then bred with CMV-Cre TG mice to obtain germline replacement of the exon containing the integrin α5 cytoplasmic domain with the integrin α2 cytoplasmic domain. (**b**) A genomic DNA fragment from homozygous knock-in mice containing the integrin α5 tail was amplified by PCR and sequenced. (**c**) Validation of integrin chimaera knock-in mouse. Lung homogenates from WT and chimaera knock-in mice were western blotted with the indicated antibodies. (**d**,**e**) Endothelial cells isolated from adult WT or chimaera knock-in homozygous mice were replated on dishes coated with poly-L-lysine or FN (10 μg ml^{-1}). (**d**) After 15 min, adherent cells were quantified using the acid phosphatase assay and normalized to the cells attached on PLL (n = 3 independent experiments). Error bars are s.e.m. (**e**) Cell spreading at the indicated times was determined as described in Methods. For each condition, n= 20 images (~10 cells per field) were pooled across three independent experiments. The box plot shows the median, with upper and lower percentiles, and the bars show maxima and minima values. Source data for **d** are available in Supplementary Table 1. (**f**) Inflammatory markers in an athero-prone artery segment of knock-in mice. Aortae from WT and chimaera knock-in homozygous mice were stained for the indicated proteins and the lesser curvature of the arch was examined. Staining intensity was quantified as described in Methods (n = 5 mice for each type). L, lumen. Data are

represented as means ± s.e.m. $^{*}P < 0.05$ by two-tailed *t*-test. Quantification data from individual mice are provided in Supplementary Table 1.

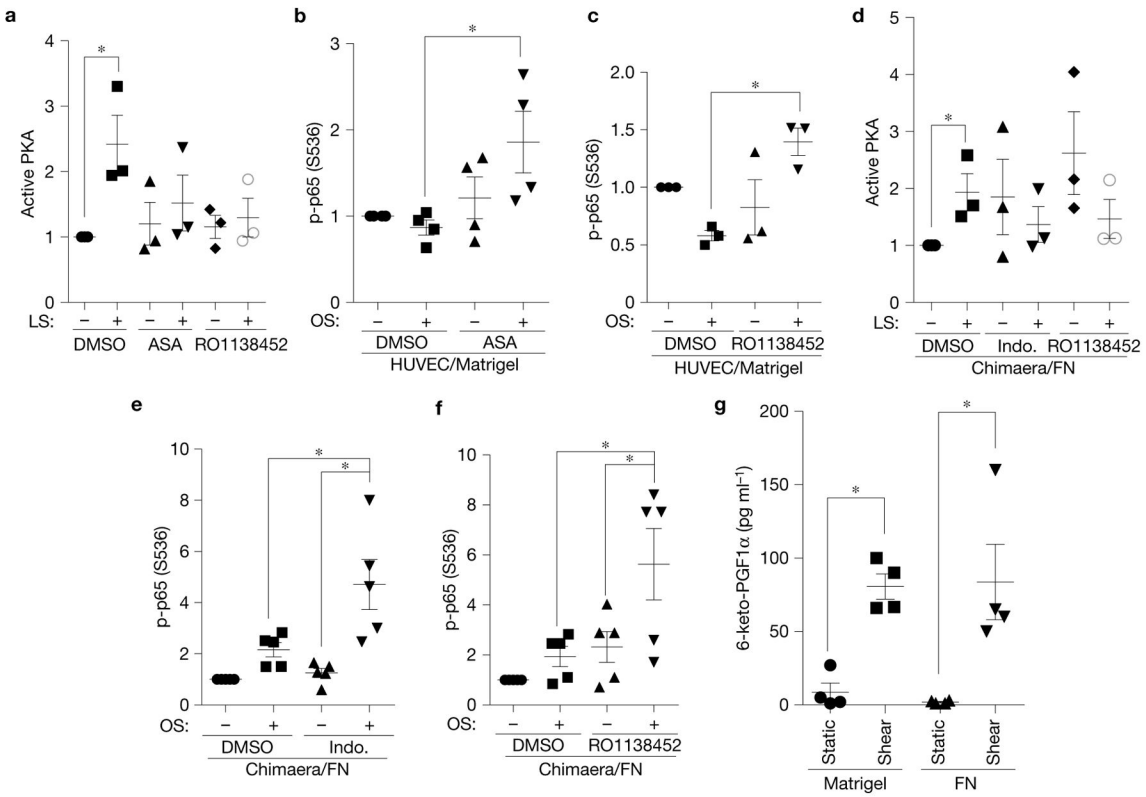

Figure 3.

Prostacyclin mediates shear-dependent PKA activation but is ECM-independent. (**a**) HUVECs on Matrigel were pretreated with aspirin (ASA, a COX inhibitor, 10 μM) or a prostacyclin receptor antagonist (RO1138452, 100 nM) and then sheared for 15 min. PKA activity was measured as in Fig. 1 ($n = 3$). LS, laminar shear; OS, oscillatory shear. (**b**,**c**) HUVECs on Matrigel pretreated with aspirin (10 μM) or RO1138452 (100 nM) were exposed to oscillatory shear for 18 h, and then NF-κB Ser536 phosphorylation was measured by western blotting. (**b**, $n = 4$; **c**, $n = 3$). (**d**) α5/2 chimaera-expressing BAECs on FN were treated with indometacin (Indo.) (10 μM) or RO1138452 (100 nM), and then sheared for 15 min. PKA activity was measured as in **a** ($n = 3$). (**e**,**f**) α5/2 chimaera cells on FN pretreated with indometacin (10 μM) or RO1138452 (100 nM) were exposed to oscillatory shear for 18 h. NF-κB activation was measured as in **b** and **c** ($n = 5$). (**g**) HUVECs on Matrigel or FN were subjected to pulsatile shear (15 dynescm^{-2} ± 5 dynescm^{-2}) for 90 min. 6-keto-PGFα in the medium was measured by ELISA ($n = 4$). Data are represented as means ± s.e.m. $^{*}P < 0.05$ by one-way ANOVA (**b**,**c**,**e**,**f**) or two-tailed t-test (**a**,**d**,**g**). In all panels n values represent independent experiments. Source data are provided in Supplementary Table 1.

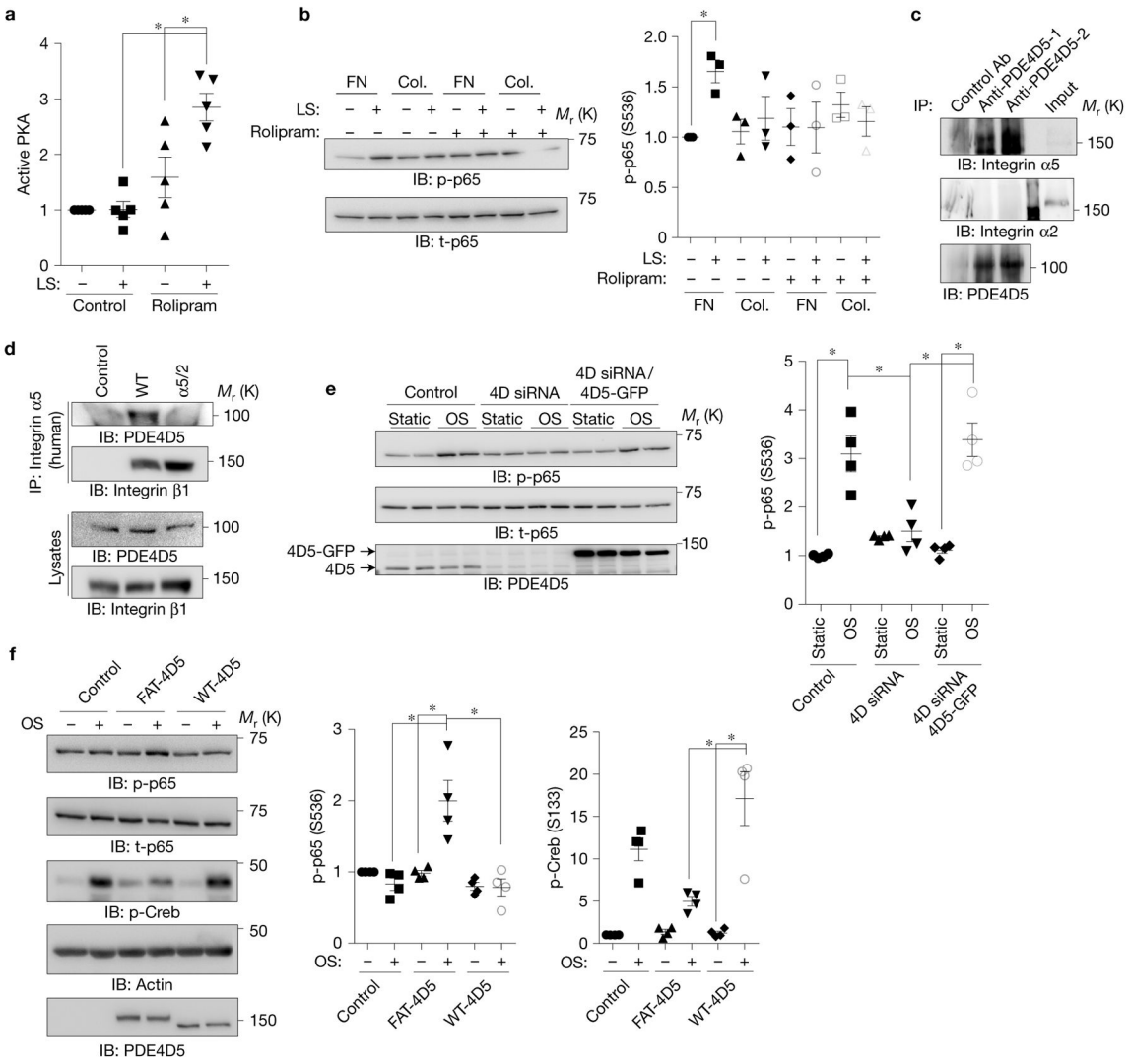

Figure 4.

Involvement of PDE4D in ECM-dependent inflammatory signalling. (**a**) BAECs on FN were treated with the PDE4 inhibitor rolipram (1 μM), sheared, and PKA activity assayed as in Fig. 1. (n = 5). (**b**) BAECs on FN or collagen (Col.) were treated with rolipram (1 μM) and assayed for NF-κB as before (n = 3). (**c**) HUVEC lysates were immunoprecipitated with two different PDE4D5 antibodies and western blots probed for integrin α5 or integrin α2. Similar results were obtained in three experiments. (**d**) BAECs expressing WT integrin α5 or the α5/2 chimaera were immunoprecipitated with human-specific integrin α5 antibody recognizing the extracellular region. Western blots were probed for PDE4D5 and for the integrin β1 subunit. Similar results were obtained in 4 experiments. (**e**) BAECs were transfected with siRNA against PDE4D and then rescued with control or PDE4D5-GFP retrovirus. Cells were subjected to oscillatory shear and NF-κB assayed as before (n = 4). (**f**) BAECs expressing WT PDE4D5 or FAT-PDE4D5 were plated on Matrigel for 5 h and subjected to oscillatory shear. NF-κB Ser536 phosphorylation and Creb Ser133 phosphorylation were measured by western blotting (n= 4). Data are represented as means ±

s.e.m. $^{*}P < 0.05$ by one-way ANOVA (**a**,**e**,**f**) or two-tailed *t*-test (**b**). In all panels *n* values represent independent experiments. Source data are provided in Supplementary Table 1. Unprocessed scans of blots are shown in Supplementary Fig. 6.

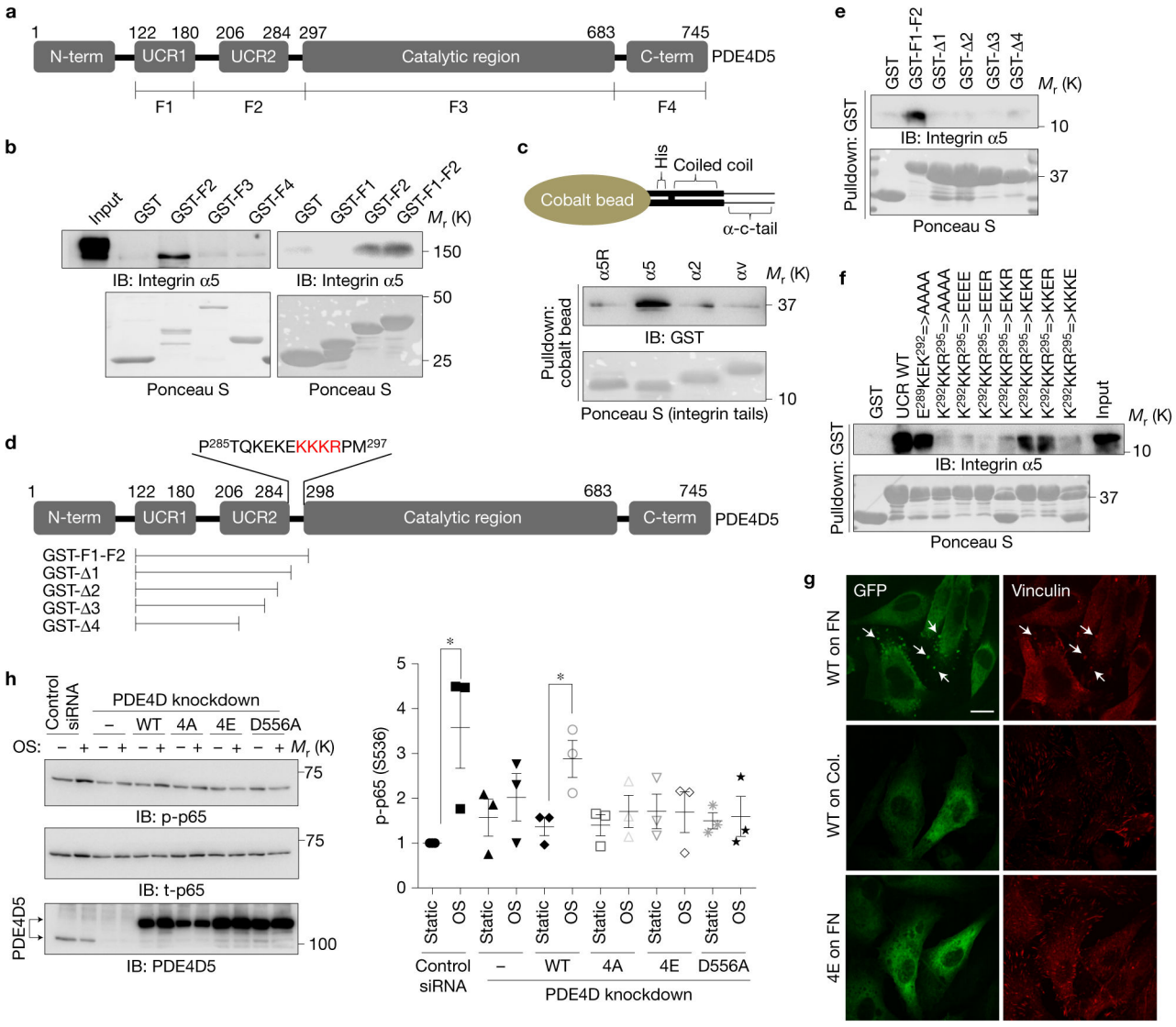

Figure 5.

Mapping the integrin binding site on PDE4D5. (**a**) Schematic representation of PDE4D5 and fragments used for pulldown assays. (**b**) HUVEC lysates were incubated with GST-tagged fragments of PDE4D5 and probed for integrin α5. Results are representative of three independent experiments. (**c**) To test whether the interaction is direct, integrin α tails immobilized on cobalt beads were incubated with purified PDE4D5 F2 fragment. Beads were washed and bound material was analysed by western blotting (α5R: scrambled sequence of α5 tail). (**d**) Deletion constructs used for detailed mapping and critical residues for binding. (**e**,**f**) The indicated PDE4D5 fragments and mutants were immobilized on GSH beads and incubated with the α5 tail protein used in **c**. Bound α5 tail protein was detected by western blotting with integrin α5 antibody against cytoplasmic tail. Results are representative of three independent experiments. (**g**) BAECs expressing GFP-tagged PDE4D5 WT or the 4E mutant were plated on FN or collagen and sheared for 15 min. The cells were fixed and stained for the focal adhesion marker, vinculin. Arrow indicates

colocalization of PDE4D5 with vinculin. Results are representative of three independent experiments. Scale bar, 50 μm. (**h**) BAECs stably expressing integrin α5 binding-deficient PDE4D5 mutants (4A and 4E) or the catalytically inactive mutant (D556A) were transfected with siRNA to knock down the endogenous PDE4D, and then were subjected to oscillatory shear for 18 h. NF-κB activity was assayed as in Fig. 1; (n= 3 independent experiments). Data are represented as means ± s.e.m. $^{*}P < 0.05$ by two-tailed t-test. Source data are provided in Supplementary Table 1. Unprocessed scans of blots are shown in Supplementary Fig. 6.

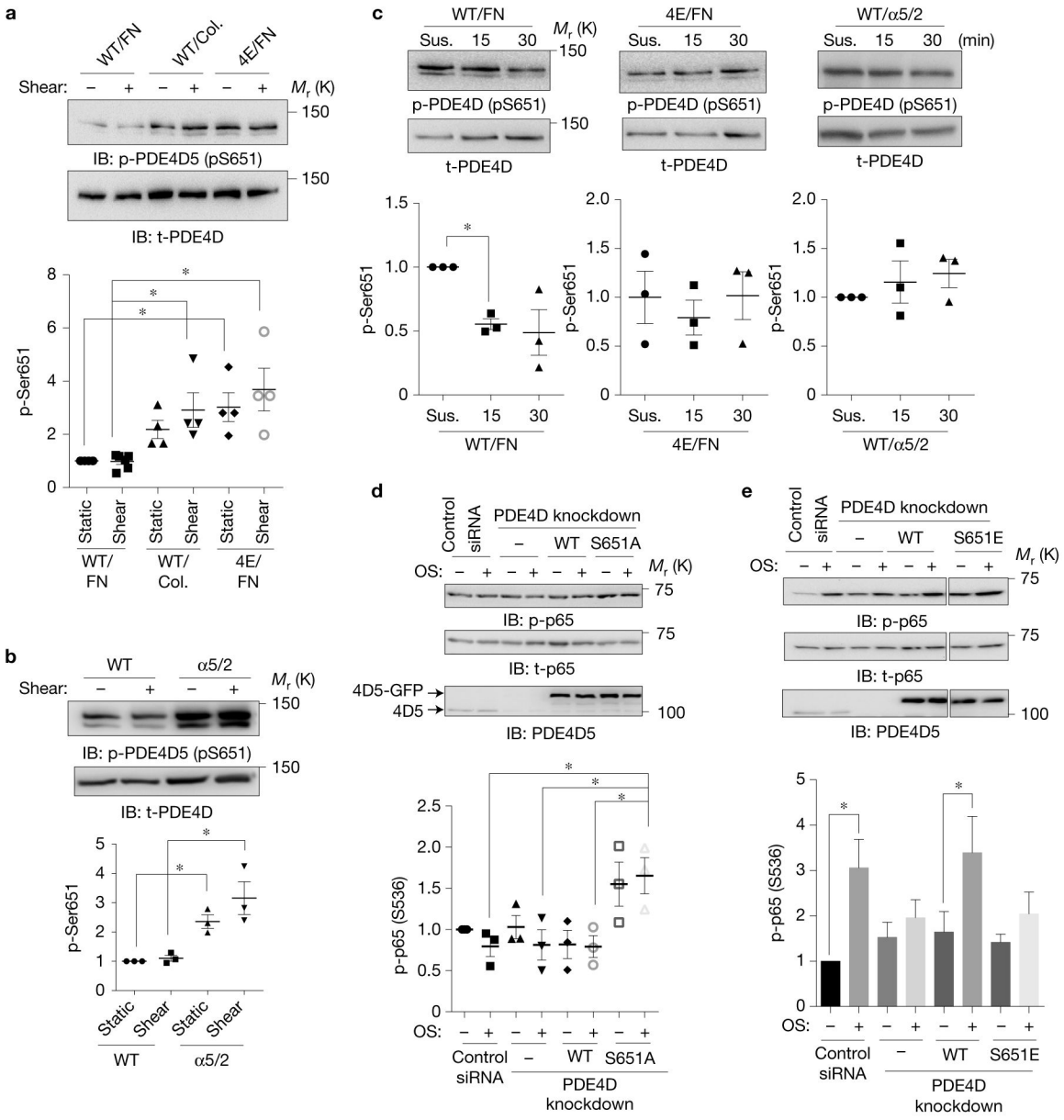

Figure 6.

ECM-dependent regulation of PDE4D phosphorylation. (**a**) BAECs expressing WT or the 4E mutant of PDE4D5 were plated on collagen or FN for 5 h and then sheared for 15 min. Cell lysates were probed for anti-pSer651-PDE4D (n = 4–6). *Y* axis values throughout the figure represent the fold change (relative to control). t-PDE4D, total PDE4D. (**b**) BAECs expressing WT integrin α5 or the α5/2 chimaera on FN were transfected with PDE4D5, and then sheared for 15 min. Ser651 phosphorylation was assayed by western blotting as in **a** (n= 3). (**c**) BAECs expressing PDE4D5 WT or the 4E mutant or chimaera cells expressing PDE4D5 WT were kept in suspension (Sus.) for 90 min and then replated on FN-coated dishes for the indicated times. Ser651 phosphorylation was assayed by western blotting (n = 3). (**d**,**e**) BAECs in which endogenous PDE4D5 was knocked down were reconstituted with

WT, phospho-deficient S651A or phospho-mimetic S651E mutants. The cells were replated on collagen (**d**) ($n = 3$) or FN (**e**) ($n = 6$) and then subjected to oscillatory shear for 2 h. NF-κB activity was assayed as in Fig. 1. In all panels n values represent independent experiments. Data are represented as means ± s.e.m. $^{*}P < 0.05$ by one-way ANOVA (**a**,**b**,**d**) or two-tailed t-test (**c**,**e**). Source data are provided in Supplementary Table 1. Unprocessed scans of blots are shown in Supplementary Fig. 6.

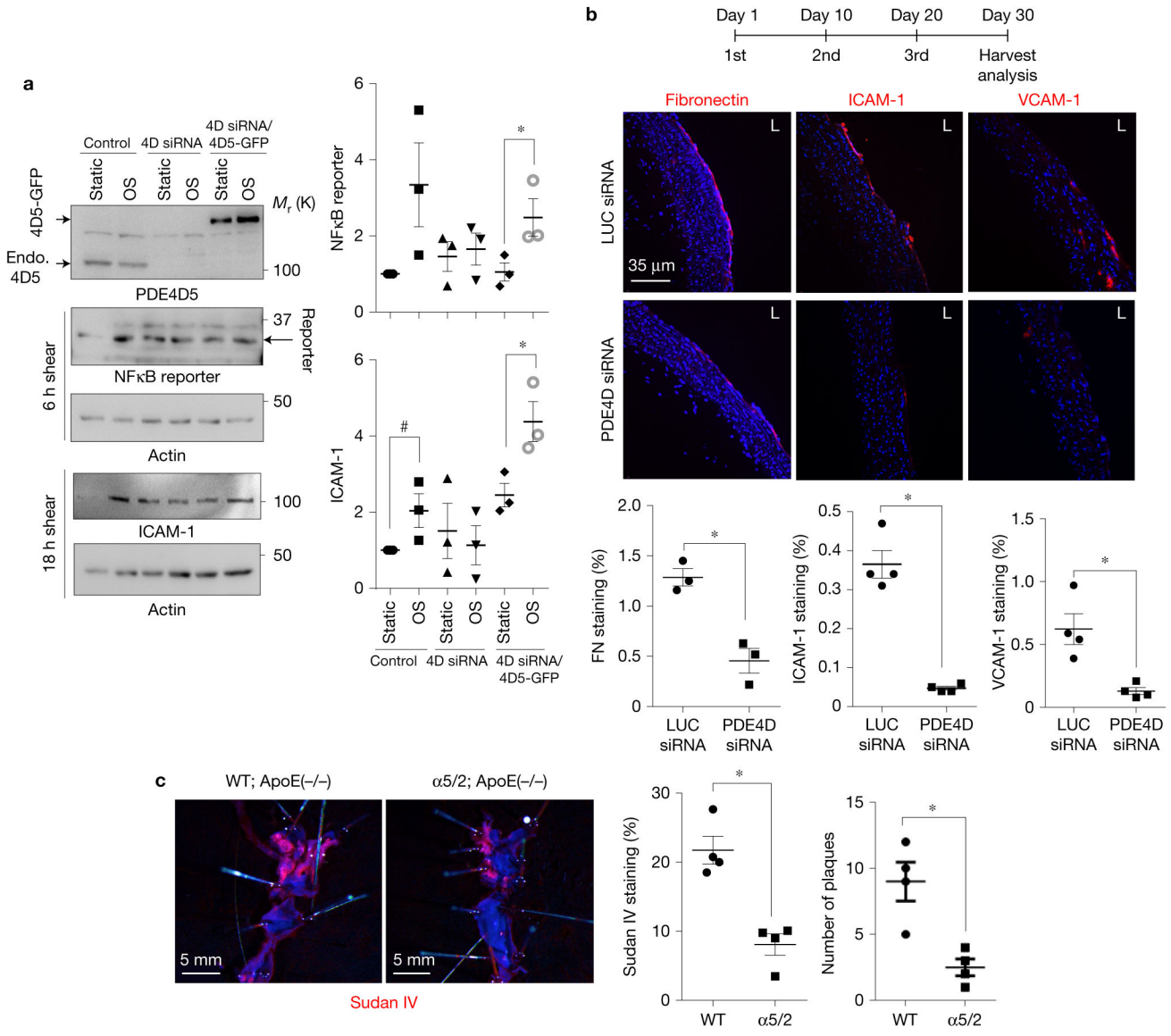

Figure 7.

In vivo PDE4D knockdown reduces flow-dependent inflammation. (**a**) Validation of siRNA used for *in vivo* knockdown. Immortalized mouse aortic endothelial cells were transfected with GFP-tagged human PDE4D5 and transfected with siRNA used for nanoparticle formulation. Endo., endogenous PDE4D5. NF-κB activation was assayed either by measuring GFP reporter expression under control of the NF-κB responsive element or ICAM-1 induction. *Y* axis values represent the fold change (relative to control). Data are represented as means ± s.e.m. $^{*}P < 0.05$ and $^{\#}P = 0.079$ by two-tailed *t*-test. ($n = 3$ independent experiments) Source data are provided in Supplementary Table 1. (**b**) Nanoparticles containing PDE4D siRNA or luciferase (LUC) siRNA (1 mg kg^{-1}) were injected intravenously. Aortae from treated mice were isolated and stained for the indicated molecules to assay inflammatory markers in lesser curvature ($n = 5$ mice). (**c**) Integrin chimaera knock-in mice were bred with ApoE null mice and fed a high-fat diet for 4 months.

Aortae were opened and stained *en face* with Sudan IV (n= 4 mice). Plaque area and numbers were quantified. Data are represented as means ± s.e.m. $^{*}P < 0.05$ by two-tailed t-test. Quantification data from individual mice are provided in Supplementary Table 1.